Physics and Chemistry of Minerals (2024) 51:36
https://doi.org/10.1007/s00269-024-01296-3

ORIGINAL PAPER

# High pressure behavior of K-cymrite ($KAlSi_3O_8 \cdot H_2O$) crystal structure

**Alexandr V. Romanenko[1] · Sergey V. Rashchenko[1,2] · Andrey V. Korsakov[1] · Alexander G. Sokol[1]**

Received: 14 May 2024 / Accepted: 1 August 2024 / Published online: 30 August 2024


**Abstract**
Compressibility and structural evolution of K-cymrite, hexagonal high-pressure $KAlSi_3O_8 \cdot H_2O$, has been studied up to 18 GPa using synchrotron single crystal X-ray diffraction in Ne pressure medium. K-cymrite retains its original symmetry *P6/mmm* up to a pressure of 7.3 GPa. As the pressure increases from 7.3 to 8.5 GPa, the weak satellite reflections appear on diffraction patterns and remain up to maximum applied pressure of 18 GPa indicating incommensurate modulation. However, main reflections can be still indexed in hexagonal cell and structure successfully solved in initial *P6/mmm* group. After pressure release, K-cymrite reverts to initial non-modulated single-crystal state. The parameters of third-order Birch-Murnaghan equation of state for K-cymrite are $V_0 = 190.45(12)$ Å$^3$, $K_0 = 56.5(7)$ GPa and $K_0' = 3.2(12)$, with bulk modulus notably deviating from earlier result ($K_0 = 45(2)$ GPa and $K_0' = 1.3(10)$) obtained in vaseline media.

**Keywords** K-cymrite · High-pressure · Single crystal synchrotron x-ray diffraction · Inconsummerate modulation · Diamond anvil cell

## Introduction

K-cymrite is a hexagonal high-pressure polymorph of $KAlSi_3O_8 \cdot H_2O$ (*P6/mmm*, $a = 5.3361(3)$ Å, $c = 7.7081(7)$ Å (Romanenko et al. 2021) which crystallizes at temperatures and pressures above 400 °C and 2.3 GPa in the $KAlSi_3O_8$-$H_2O$ system (Seki and Kennedy 1964; Massonne 1992; Fasshauer et al. 1997; Thompson et al. 1998). Thompson et al. (Thompson et al. 1998) obtained a dehydrated form by heating K-cymrite up to 800 °C at ambient pressure, which was later found in nature and approved as the mineral kokchetavite (IMA-2004-011).

The structure of K-cymrite consists of double tetrahedral layers $[(Al, Si)_2O_5]_{2\infty}$ with no NMR evidence of Al/Si ordering (Fasshauer et al. 1997; Kanzaki et al. 2012), linked through bridging oxygen atoms and alternating with layers of $K^+$ cations (Fig. 1). The double layers form six-membered rings with enclosed voids occupied by $H_2O$ molecules disordered along the *c* axis (Fig. 1).

Among phases with the same structure topology, such as kokchetavite ($KAlSi_3O_8$), dmisteinbergite ($Ca_2Al_2Si_2O_8$), hexacelsian $BaAl_2Si_2O_8$, $SrAl_2Si_2O_8$, cymrite $BaAl_2Si_2O_8 \cdot H_2O$ (Takeuchi and Donnay 1959; Dimitrijević et al. 1997; Bolotina et al. 2010; Zolotarev et al. 2019; Romanenko et al. 2021), K-cymrite has the highest possible symmetry due to the Al/Si disorder and the absence of ditrigonal rotation of $SiO_4$ tetrahedra. The latter is attributed to large size of $K^+$ cations and the presence of water restricting the ditritogonal deformation of the double tetrahedral rings (Krivovichev 2020).

According to calculated pseudosections ($P = 0.3$–$2.8$ GPa, $T = 250$–$650$ °C) for metagranites from the Gran Paradiso Massif under $H_2O$-saturated conditions, K-cymrite replaces K-feldspar at pressures exceeding approximately 2 GPa (Massonne 2015). In pseudosections for greater depths ($P = 4$–$15$ GPa, $T = 700$–$1500$ °C) for fluid-saturated crust, K-cymrite demonstrates stability between 6.5 and 10 GPa along a warm geotherm (Chapman et al. 2019). Recent experimental studies by Sokol et al. (Sokol et al. 2020, 2023) with nitrogen-bearing pelitic systems at pressures of 6.3–7.8 GPa revealed that K-cymrite can incorporate up to 5 wt% of nitrogen into its structure, suggesting its role as nitrogen transporter into the mantle.

✉ Alexandr V. Romanenko
romanenko.alxndr@gmail.com

[1] Sobolev Institute of Geology and Mineralogy SB RAS, 3 Koptyuga Avenue, Novosibirsk 630090, Russia

[2] Novosibirsk State University, 2 Pirogova Street, Novosibirsk 630090, Russia

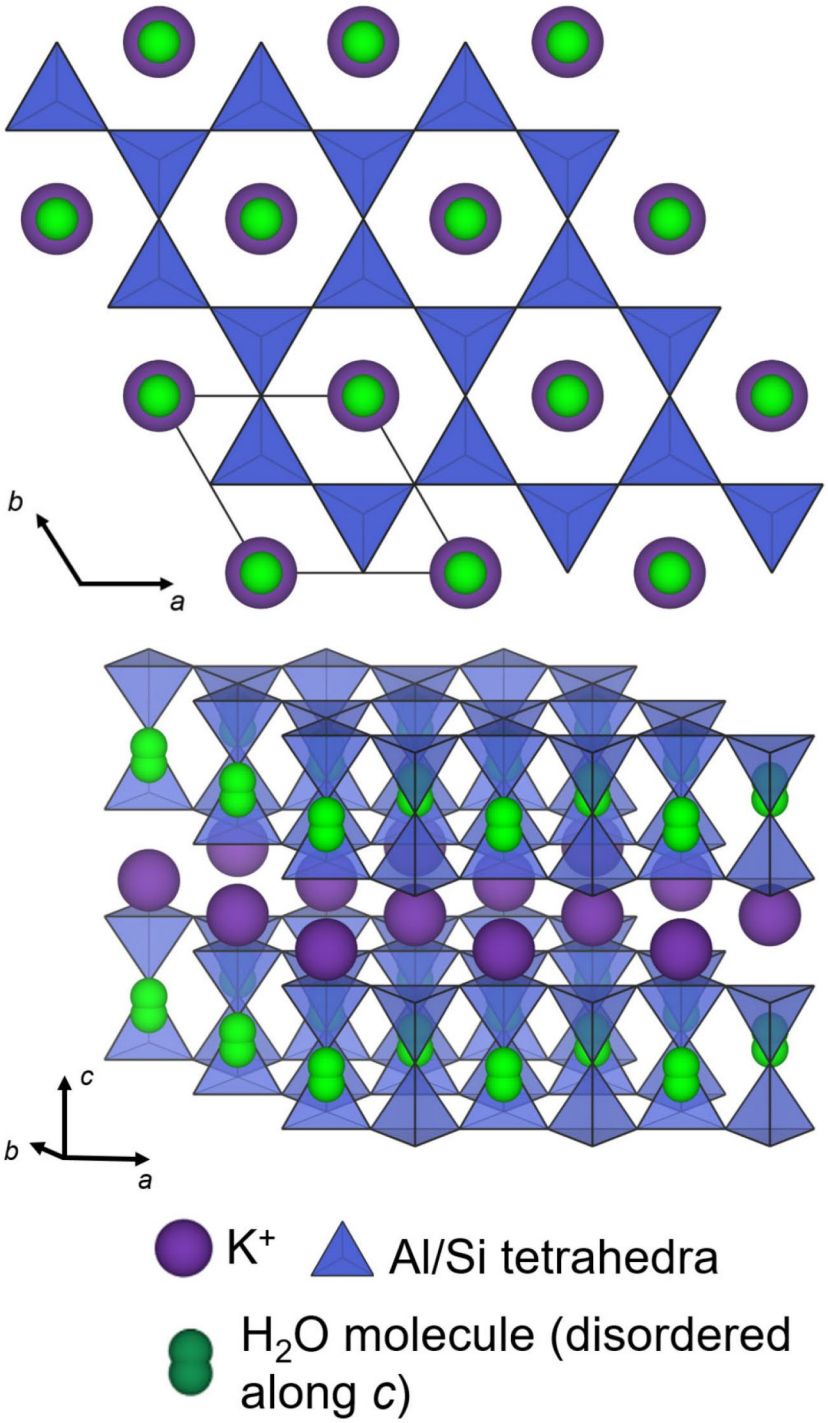


**Fig. 1** Projection of K-cymrite structure along the [001] direction (**a**); perspective view of the K-cymrite structure (**b**). The large spheres represent the interlayer K-atoms, and the smaller ones are disordered $H_2O$ molecules in the cages inside the double tetrahedral layers

To date, only one finding of K-cymrite coexisting with kokchetavite in polyphase mineral inclusions has been reported (Mikhno et al. 2013). However, the dehydrated form of K-cymrite – kokchetavite $KAlSi_3O_8$ has been found in numerous mineral inclusions across various regions, including the Kokchetav and Bohemian massifs, the Ivrea Zone (NW Italy), the Gruf Complex (European Central Alps), eastern Papua New Guinea (U)HP terrane, and the Kangerlussuaq basement (Southeast Greenland) (Hwang et al. 2013; Mikhno et al. 2013; Ferrero et al. 2016; Carvalho et al. 2019; Borghini et al. 2020; Gianola et al. 2020; Schönig et al. 2020; Baldwin et al. 2021; Nicoli et al. 2022; Wannhoff et al. 2022), as well as in garnets of shock-induced melt veins of amphibolite clasts (Ståhle et al. 2022). Nevertheless, the origin of kokchetavite in these inclusions remains a subject of debate. While most interpretations suggest direct

metastable crystallization from the trapped melt, regardless of internal pressure or specific conditions of melt entrapment, some authors propose that kokchetavite crystallizes through the dehydration of the K-cymrite precursor (Hwang et al. 2004).

The high-pressure behavior of K-cymrite was first studied by Fasshauer et al. (Fasshauer et al. 1997) up to 6 GPa using powder X-ray diffraction in vaseline as a pressure medium. However, vaseline exhibits a high degree of non-hydrostaticity at such pressures and room temperature, potentially leading to errors in determining the bulk modulus. Since the equation of state of K-cymrite is used in thermodynamic modeling of fluid-saturated crust, it necessitates refinement under more hydrostatic conditions and at higher pressures.

Here, the high-pressure behavior of K-cymrite was studied at room temperature by in situ single-crystal synchrotron X-ray diffraction in Ne pressure medium up to 18 GPa and by Raman spectroscopy in methanol-ethanol pressure medium up to 12 GPa.

## Experimental

### Synthesis

K-cymrite was obtained in high-pressure experiment at 6.3 GPa and 1000 °C using $KAlSi_3O_8$ glass-ceramics and liquid water in stoichiometric proportion as starting materials. The details of high-pressure cell assemblage and experimental description are given in Romanenko et al. (2021).

### Chemical composition

The composition of obtained K-cymrite was investigated using a MIRA 3 LMU scanning electron microscope (Tescan Orsay Holding, 20 kV accelerating voltage and 1.5 nA beam current) coupled with an INCA 450 energy-dispersive X-ray microanalysis system equipped with a liquid nitrogen-free large area EDS X-Max-80 Silicon Drift Detector (Oxford Instruments Nanoanalysis Ltd) at IGM SB RAS.

The average of 33 analyses of 8 grains of the K-cymrite is: $SiO_2$ 61(1.3) wt%, $Al_2O_3$ 17.1(5) wt%, $K_2O$ 15.3(3) wt% (sum 93.59% wt%). After normalizing to eight oxygens, we obtained the following formula: $K_{0.96(2)}Al_{1.01(1)}Si_{3.01(1)}O_8 \cdot H_2O$. We did not observe any variations of chemical composition between different grains and inhomogeneities across a grain exceeding the measurement error.

#### Synchrotron single-crystal X-ray diffraction at high pressure

The crystal selection and diffraction data collection were performed at P02.2 beamline of PETRA III, Deutsches Elektronen-Synchrotron (DESY) (Liermann et al. 2015). X-ray diffraction measurements were performed at a wavelength of 0.2897 Å (42.7 keV) with a beam size as of $8 \times 3$ $\mu m^2$ at the focal spot. Neon was used as a pressure medium. The crystal of K-cymrite approximately of $0.05 \times 0.04 \times 0.03$ $mm^3$ were placed into membrane driven symmetric diamond anvil cell (DAC), equipped with Boehler-Almax anvils (400 µm culet size). The effective conical aperture of the DACs was ~64°. A 250 µm rhenium foil was used as the gasket material, indented to a thickness of ~80 µm. The indentation area was drilled in the center to produce a sample chamber with diameter of 140 µm. Pressure was determined using ruby fluorescence scale (Shen et al. 2020).

Diffraction patterns were collected using the fast area detector XRD 1621 (PerkinElmer) during ±30° rotation of the diamond anvil cell. For each pressure point, two datasets were acquired with different exposures (ω scan, scan step 0.5°, exposure 3 and 0.5 s per frame).

The patterns were then transferred into CrysAlisPro software using the ESPERANTO protocol (Rothkirch et al. 2013) for indexing and integration. The structure was solved by SHELXT method in *P6/mmm* space group and refined using the Jana2020 program package (Petříček et al. 2014; Sheldrick 2015). An overview of the data and refinement results are listed in Table 1 (see also a supplementary CIF). At low exposure (0.5 s) some of the weak reflections have insufficient intensity and, at the same time, at high exposure (3 s) some of the reflections are overexposed. So, the refinement was performed using two datasetes at both exposures of 3 and 0.5 s for each pressure point.

The crystal structure of compressed K-cymrite was solved and refined at multiple pressure points within anisotropic displacement approximation for K-atoms and isotropic for the rest. Weak satellite reflections appeared at pressures above 7.3 GPa were ignored and main reflections used for structure refinement in the *P6/mmm* space group. The refined structures between 8.5 and 17.6 GPa therefore approximate 'average' structures in terms of incommensurate crystallography.

### High pressure Raman spectroscopy of K-cymrite

Raman spectra of K-cymrite were studied up to 12 GPa using diamond anvil cell technique (Mao–Bell type) (Fursenko et al. 1986). The crystal of K-cymrite approximately of $0.07 \times 0.04 \times 0.03$ $mm^3$ was placed into diamond anvil cell (DAC) (600 µm culet size). A 300 µm tungsten foil was used as the gasket material, indented to a thickness of ~80 µm. The indentation area was drilled in the center to produce a sample chamber with diameter of 200 µm. Methanol-ethanol 4:1 mixture was used as a pressure transmitting medium and ruby as a pressure sensor (Shen et al. 2020).

**Table 1** Details of data collection and structure refinement

| *P*, GPa | Space group | a, Å | c, Å | V, Å$^3$ | $R_{int}$ | $R_1[F^2 > 2\sigma(F^2)]$, wR($F^2$), S | No. of independent reflections /Number of parameters |
|---|---|---|---|---|---|---|---|
| 0.0001 from article (Romanenko et al. 2021) | *P6/mmm* | 5.3361(3) | 7.7081(7) | 190.08(3) | 0.047 | 0.040, 0.091, 1.36 | 127/17 |
| 3.31(5) | *P6/mmm* | 5.2865(3) | 7.4310(7) | 180.56(2) | 0.052 | 0.093, 0.165, 2.00 | 130 / 11 |
| 4.54(7) | *P6/mmm* | 5.2645(3) | 7.3750(7) | 177.02(2) | 0.074 | 0.118, 0.180, 1.99 | 124 / 11 |
| 5.01(8) | *P6/mmm* | 5.2556(3) | 7.3340(7) | 176.5(2) | 0.056 | 0.124, 0.187, 2.29 | 130 / 11 |
| 7.3(19) | *P6/mmm** | 5.2163(3) | 7.2360(7) | 170.52(2) | 0.056 | 0.121, 0.176, 2.19 | 121 / 11 |
| 8.5(2) | *P6/mmm** | 5.1972(3) | 7.1160(7) | 167.63(2) | 0.053 | 0.147, 0.199, 2.45 | 125 / 11 |
| 9.7(14) | *P6/mmm** | 5.1782(3) | 7.1170(7) | 165.34(2) | 0.055 | 0.133, 0.203, 2.69 | 112 / 11 |
| 10.7(2) | *P6/mmm** | 5.1610(3) | 7.0930(7) | 163.84(2) | 0.059 | 0.137, 0.197, 2.37 | 109 / 11 |
| 12.3(2) | *P6/mmm** | 5.1374 (3) | 7.0270 (7) | 161.19 (2) | 0.062 | 0.119, 0.204, 2.42 | 106 / 11 |
| 13.5(14) | *P6/mmm** | 5.1209(3) | 6.9910(7) | 158.95(2) | 0.060 | 0.100, 0.184, 2.24 | 103 / 11 |
| 14.5(2) | *P6/mmm** | 5.0991(3) | 6.9410(7) | 156.74(2) | 0.054 | 0.099, 0.202, 2.53 | 107 / 11 |
| 16.2(18) | *P6/mmm** | 5.0814(3) | 6.9049(7) | 154.83(2) | 0.056 | 0.090, 0.189, 2.23 | 105 / 11 |
| 17.59(7) | *P6/mmm** | 5.0669(3) | 6.8818(7) | 153.64(2) | 0.048 | 0.120, 0.224, 2.30 | 109 / 11 |

*with weak satellite reflections

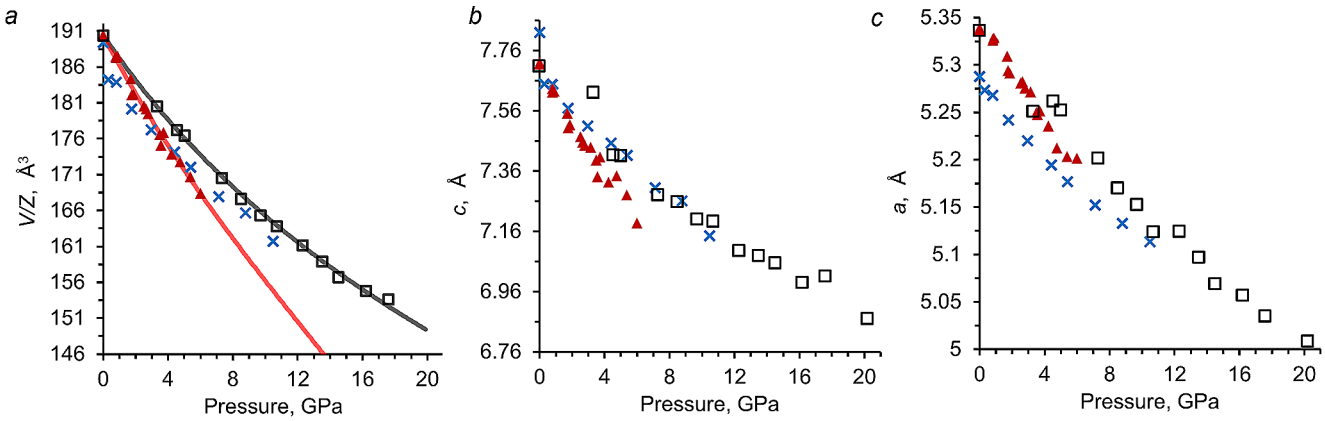


**Fig. 2** Dependence of the unit cell parameters of K-cymrite with pressure. Squares correspond to K-cymrite parameters; the gray line show the 3d order Birch-Murnaghan fit of the $V/V_0$ data points for K-cymrite; red triangles and line are from (Fasshauer et al. 1997); blue crosses are kokchetavite from (Romanenko et al. 2024). Hereafter, the e.s.d. values are slightly smaller than the size of the symbols

Raman measurements of K-cymrite ($KAlSi_3O_8 \cdot H_2O$) were performed using a Horiba Jobin Yvon LabRAM HR800 Raman spectrometer with a 532-nm solid state laser. Spectra were recorded at ambient conditions in backscattering geometry with a laser power of about 1 mW and a spectral resolution of approximately 2 cm$^{-1}$. The positions of Raman bands were fitted using the Voigt function in the Fityk 1.3.1 program (Wojdyr 2010).

## Results and discussion

### K-cymrite equation of state

To describe the *PV*-data of K-cymrite we use third-order Birch-Murnaghan (BM) equation of state. The dependence of the unit cell parameters of K-cymrite on pressure is shown in Fig. 2.

The parameters of third-order Birch-Murnaghan equation of state for K-cymrite are $V_0 = 190.45(12)$ Å$^3$, $K_0 = 56.5(7)$ GPa and $K_0' = 3.2(12)$ (see Table 2). The bulk modulus $K_0 = 56.5(7)$ GPa for K-cymrite obtained in this work notably deviates from the compression modulus reported by Fasshauer et al. (Fasshauer et al. 1997) ($K_0 = 45(2)$ GPa and

**Table 2** Coefficients of Birch-Murnaghan equations of state for potassium feldspar polymorphs

| | K-cymrite (Fasshauer et al. 1997) | K-cymtire (this article) | Kokchetavite-II (Romanenko et al. 2024) | Microcline (Allan and Angel 1997) | Lieber-mannite (Ferroir 2006) |
|---|---|---|---|---|---|
| $V_0/Z$, Å$^3$ | 190.29(1) | 190.45(12) | 185(4) | 179.9(3) | 105.24(1) |
| $K_0$, GPa | 45(2) | 56.5(7) | 59(2) | 58.3(2.0) | 201.4(7) |
| $K_0$' | 1.3(10) | 3.2(12) | 4.0 | 4.0 | 4.0 |

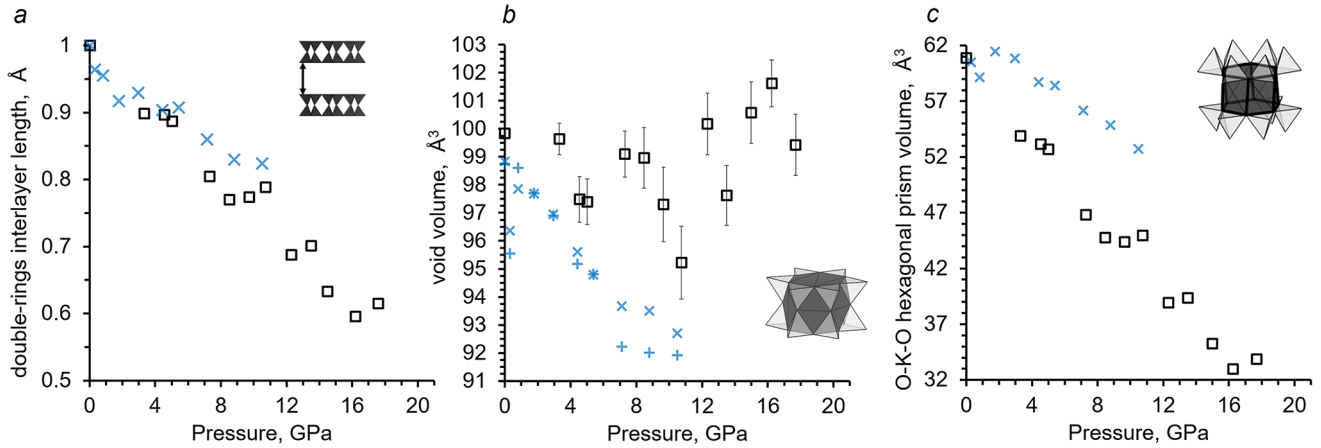


**Fig. 3** Pressure dependence of: (**a**) normalized interlayer distance; (**b**) void volume enclosed rings (see inset); (**c**) hexagonal prismvolume. Squares correspond to K-cymrite, gray crosses represent kokchetavite from Romanenko et al. (Romanenko et al. 2024)

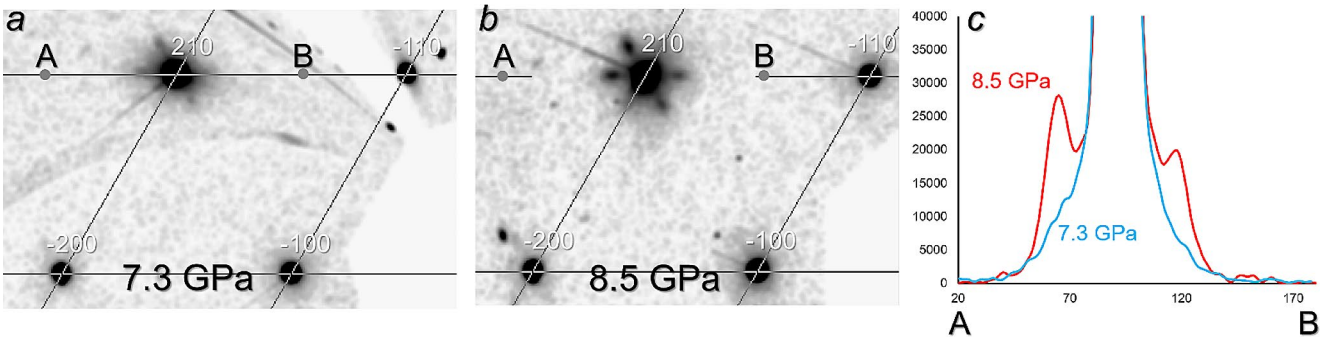


**Fig. 4** The (*hk0*) plane of the reciprocal lattice of K-cymrite at (**a**) 7.3 GPa and (**b**) 8.5 GPa; (**c**) cross-section of diffraction intensity through A-B

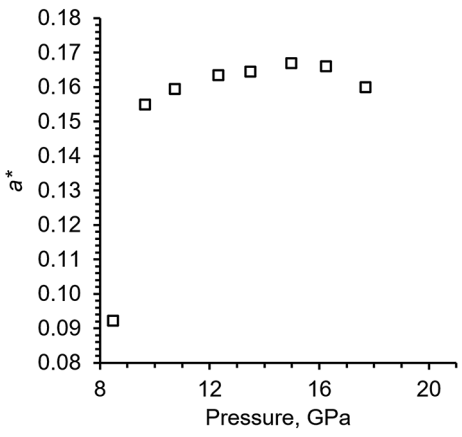


**Fig. 5** Evolution of *a** vector with pressure

$K_0$' = 1.3(10). This discrepancy is likely due to the fact that Fasshauer et al. (1997) used vaseline as a pressure-transmitting medium, which has a high degree of non-hydrostaticity. Comparison of K-cymrite bulk modulus with potassium feldspar polymorphs is listed at Table 2. Bulk modulus $K_0$ = 56.5(7) GPa is very close to that of kokchetavite (59(2) GPa) and microcline (58.3(2.0) GPa).

## High-pressure behavior of the crystal structure

The behavior of the structural elements of K-cymrite under pressure is shown in Fig. 3.

K-cymrite responds to compression without ring ditrigonalization or distortion of the Al/Si framework (Fig. 3a, 4), so that compression predominantly results in the reduction of interlayer distance (Fig. 5a). This phenomenon is

associated with the presence of $H_2O$ molecules in the structural voids, which prevents distortion of the framework.

An interesting structural feature of K-cymrite at high pressure is the absence of a reduction in the volume of the hexagonal void due to the presence of $H_2O$ molecules (Fig. 3b). Since the shape of the rings does not change with pressure, the coordination of potassium with oxygen of the rings remains a regular hexagonal prism, with volume uniformly decreasing with increasing pressure (Fig. 3b). However, while under atmospheric pressure the K–Ow distance (3.557(14) Å) is noticeably longer than the length of the potassium bond with ring oxygens (3.1348(17) Å), starting from the first applied pressure (3.3 GPa) the K–Ow bond length (2.89(4) Å) becomes comparable to the K–O distance (3.031(7) Å) (Supplementary Figure S1). The latter indicates a change in potassium coordination towards a capped hexagonal prism.

## Incommensurate modulation

With a pressure increase from 7.3 to 8.5 GPa the weak satellite reflections appear on diffraction patterns and remain up to maximum applied pressure of 17.6 GPa indicating incommensurate modulation (Fig. 4). With a pressure increase from 7.3 GPa to 8.5 GPa, the modulation vector substantially increases from 0.09a* to 0.15a*, and remains in the range of 0.155–0.165 with a maximum at 14.5 GPa (Fig. 5). In addition, positions of the satellite reflections suggest the presence of twinning with three or six components of an incommensurately modulated phase with a pseudo-hexagonal cell.

A similar phenomenon was described for cymrite $Ba_2Al_2Si_2O_8{\cdot}H_2O$ at atmospheric pressure (Bolotina et al. 2010). In case of $Ba_2Al_2Si_2O_8{\cdot}H_2O$ cymrite, the appearance of modulation is caused by wave-like puckering of double tetrahedral layers, as well as ordering of $H_2O$ molecules in cavity along the modulation vector. We assume the same phenomenon takes place in K-cymrite being associated with the structure response to compression.

## Comparison with kokchetavite high-pressure behavior

The pressure-induced structural changes of kokchetavite were investigated up to 11.8 GPa by Romanenko et al. (2024) (Romanenko et al. 2024). The study identified phase transitions at pressures of 0.3 and 10.4 GPa. During the first phase transition, the symmetry changes from *P*6/*mcc* space group to the $p\overline{6}c2$, resulting in distorted hexagonal rings and a contraction in the *c* parameter. Subsequently, as pressure increased beyond 10.4 GPa, another phase transition occurred, characterized by the appearance of satellite reflections indicating structural modulation. Upon decompression, kokchetavite reverted to its initial state, suggesting the preservation of its topology despite structural transformations.

Unlike the structural changes observed in kokchetavite, where the primary response to compression is ditrigonalization of the rings, K-cymrite responds to compression without ring ditrigonalization or distortion of the Al/Si framework. Another notable difference is that in kokchetavite, the ditrigonalization of the rings leads to non-equivalent K–O bonds lengths, resulting in a change in the coordination of $K^+$ from hexagonal prism to octahedron. Whereas in K-cymrite, the hexagonal rings maintain their geometry, 12 bonds of $K^+$ with oxygens of framework remaining equivalent. Moreover, $K^+$ changes to a capped prism due to the decreasing K-Ow length and bond formation.

## High pressure Raman spectroscopy of K-cymrite

At ambient conditions, the Raman modes of K-cymrite exhibit peaks at 115 $cm^{-1}$, 382 $cm^{-1}$, and 833 $cm^{-1}$, accompanied by weaker and broader bands at 1066 $cm^{-1}$ and 1109 $cm^{-1}$. Peaks attributed to $H_2O$ molecules are observed at 1602 $cm^{-1}$ (bending mode), 3546 $cm^{-1}$ ($v_1$, symmetric stretching mode), and 3620 $cm^{-1}$ ($v_3$, antisymmetric stretching mode). Raman spectra of K-cymrite were measured up to 12 GPa, covering the OH region (Fig. 6).

The positions of the most intense Raman bands (382 and 833 $cm^{-1}$ at atmospheric pressure) of K-cymrite gradually shift toward higher wavenumbers with increasing pressure (Fig. 6). We observe the splitting of the 833 $cm^{-1}$ line into a doublet between pressures of 4.8 and 5.15 GPa (Fig. 6a). Apparently, it is associated with the appearance of incommensurate modulation. Calculated $v_0$, pressure-induced shift ($dv/dP$, $cm^{-1}$/GPa) and Gruneisen parameters of K-cymrite Raman bands are listed in Table 3.

Pressure-induced shift of 382 $cm^{-1}$ Raman band is generally agrees with earlier data reported by Kanzaki et al. (Kanzaki et al. 2012) for the same pressure medium. The OH band shows an anomalous shift from 3545 to 3541 $cm^{-1}$ between 1 atm and 2 GPa, and then an opposite shift back to 3545 $cm^{-1}$ between 2 and 4 GPa. Interestingly, during further compression from 4 to 12 GPa, position of K-cymirite OH-band (3545 $cm^{-1}$) is pressure-independent (Fig. 6). The same position of this band at ambient pressure and in the 4–12 GPa region is consistent with pressure-independent volume of structural void which hosts $H_2O$ molecule (Fig. 5). An excursion of K-cymirite OH-band towards lower wavenumbers and back during compression up to 4 GPa is probably related to reconfiguration of H-bond system caused by appearance of new K–Ow bonds.

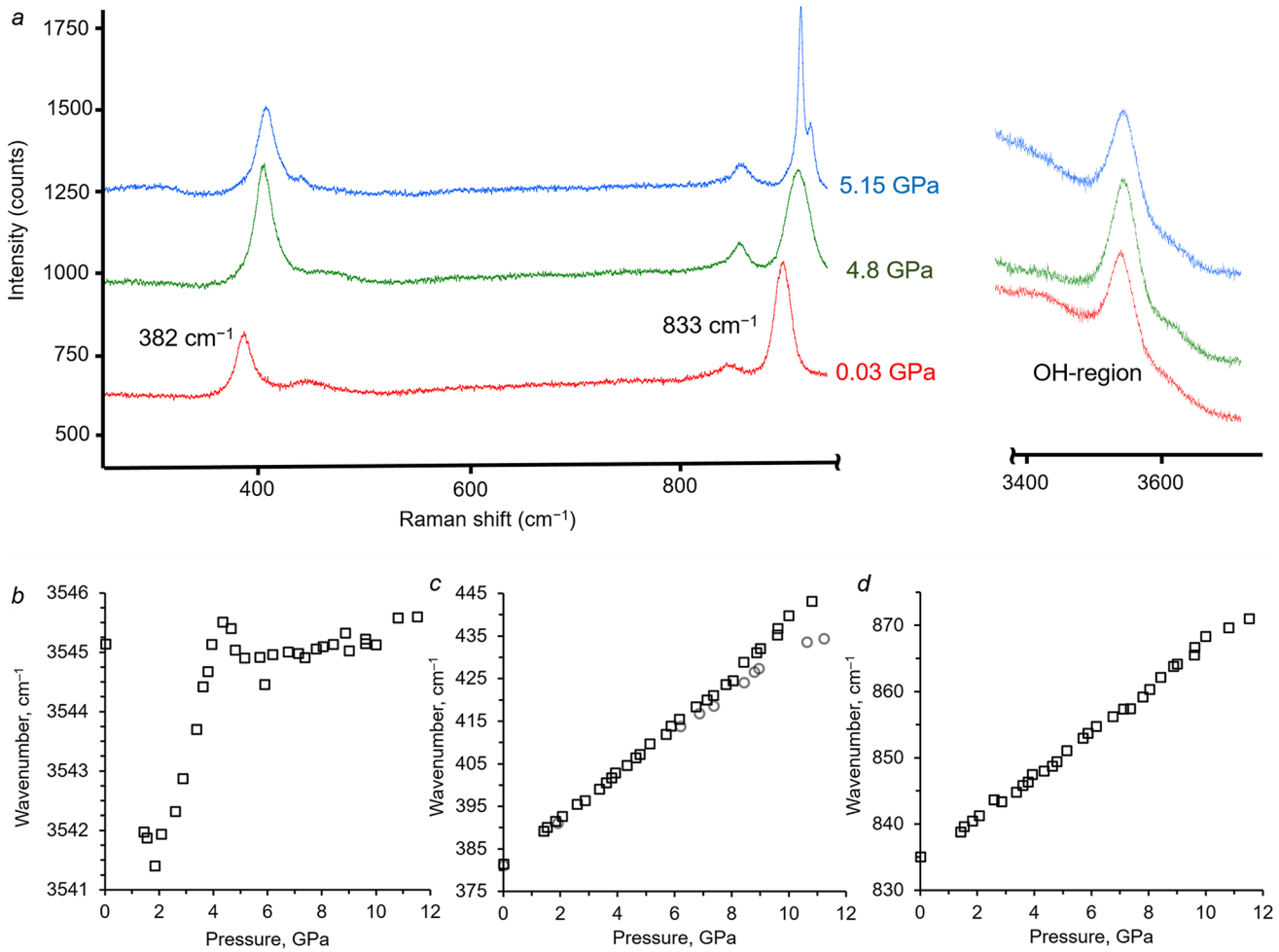


**Fig. 6** (**a**) Raman spectra of K-cymrite at 0.03, 4.8 and 5.15 GPa ; (**b**) pressure induced-shift ofOH-region; (**c**) 382 $cm^{-1}$ band (grey dots the data of (Kanzaki et al. 2012); (**d**) 833 $cm^{-1}$ band

**Table 3** Calculated $v_0$, pressure-induced shift (d$v$/d$P$, $cm^{-1}$/GPa) and Gruneisen parameters of K-cymrite bands

| | | $v_0$, $cm^{-1}$ | dv/dP, $cm^{-1}$/GPa | $\gamma_0$ |
|---|---|---|---|---|
| 382 $cm^{-1}$ | 0–8 GPa | 381.2(17) | 5.42(4) | 0.80(3) |
| | 8–12 GPa | | 5.67(9) | |
| 833 $cm^{-1}$ | 0–8 GPa | 834.5(2) | 3.17(4) | 0.215(9) |
| | 8–12 GPa | | 2.9(2) | |

## Conclusions

We do not observe phase transitions up to 18 GPa except the occurrence of satellite reflections associated with incommensurate modulation. The bulk modulus $K_0 = 56.5(7)$ GPa for K-cymrite obtained in this work notably deviates from the compression modulus obtained in the paper by Fasshauer (Fasshauer et al. 1997) ($K_0 = 45(2)$ GPa). This discrepancy is likely due to the fact that Fasshauer et al. (1997) used vaseline as a pressure transmitting medium, which has a high degree of non-hydrostaticity. Also, the anomalously low $K_0$' reported by Fassahuer appears to be a consequence of an non-hydrostaticity. Our data show that at a pressure of approximately 10 GPa, the deviation between the equation of state by Fasshauer and that obtained in this work is approximately 4 GPa, which may lead to comparable shifts of phase equilibria involving K-cymrite on phase diagrams and pseudo-sections.

**Supplementary Information** The online version contains supplementary material available at https://doi.org/10.1007/s00269-024-01296-3.

**Acknowledgements** We want to thanks Konstantin V. Glazyrin invaluable help in conducting the experiment. We acknowledge DESY (Hamburg, Germany), a member of the Helmholtz Association HGF, for the provision of experimental facilities. Parts of this research were carried out at PETRA III, P02.2 Extreme conditions beamline, proposal #I-20211603. This study is supported by the Russian Science Foundation (project 18-17-00186). A part of the work related to the study of behavior of incommensurate modulation was carried out with the support Russian Science Foundation (project 23-77-10047). A.G. Sokol work on K-cymrite synthesis was supported by the Russian Science Foundation (project 22-17-00005) and by state assignment of IGM SB RAS.

**Author contributions** Alexandr Romanenko (corresponding author) and Sergey Rashchenko wrote the main manuscript text and made all experimental work. Alexander Sokol made a high-pressure synthesis of K-cymrite. Andrey Korsakov is is responsible for the geological relevance of the article. All authors reviewed the manuscript.

**Data availability** No datasets were generated or analysed during the current study.

## Declarations

**Competing interests** The authors declare no competing interests.

## References


Allan DR, Angel RJ (1997) A high-pressure structural study of microcline (KAlSi3O8) to 7 GPa. Eur J Mineral 9:263–276

Baldwin SL, Schönig J, Gonzalez JP, Davies H, von Eynatten H (2021) Garnet sand reveals rock recycling processes in the youngest exhumed high- and ultrahigh-pressure terrane on Earth. Proceedings of the National Academy of Sciences, 118, e2017231118

Bolotina NB, Rastsvetaeva RK, Kashaev AA (2010) Refinement of the twinned structure of cymrite from the Ruby Creek deposit (Alaska). Crystallogr Rep 55:569–574

Borghini A, Ferrero S, O'Brien PJ, Laurent O, Günter C, Ziemann MA (2020) Cryptic metasomatic agent measured in situ in Variscan mantle rocks: melt inclusions in garnet of eclogite, Granulitgebirge, Germany. J Metamorph Geol 38:207–234

Carvalho BB, Bartoli O, Ferri F, Cesare B, Ferrero S, Remusat L, Capizzi LS, Poli S (2019) Anatexis and fluid regime of the deep continental crust: new clues from melt and fluid inclusions in metapelitic migmatites from Ivrea Zone (NW Italy). J Metamorph Geol 37:951–975

Chapman T, Clarke GL, Daczko NR (2019) The role of buoyancy in the fate of ultra-high-pressure eclogite. Sci Rep, 9

Dimitrijević R, Kremenović A, Dondur V, Tomašević-Čanović M, Mitrović M (1997) Thermally Induced Conversion of Sr-Exchanged LTA- and FAU-Framework Zeolites. Syntheses, Characterization, and Polymorphism of Ordered and Disordered $Sr_{1-x}Al_{2-2x}Si_{2+2x}O_8$ ($x=0$; 0.15), Diphyllosilicate, and Feldspar Phases. J Phys Chem B 101:3931–3936

Fasshauer DW, Chatterjee ND, Marler B (1997) Synthesis, structure, thermodynamic properties, and stability relations of K-cymrite, K [AlSi 3 O 8]· H 2 O. Phys Chem Miner 24:455–462

Ferrero S, Ziemann MA, Angel RJ, O'Brien PJ, Wunder B (2016) Kumdykolite, Kokchetavite, and cristobalite crystallized in nanogranites from felsic granulites, Orlica-Snieznik Dome (Bohemian Massif): not evidence for ultrahigh-pressure conditions. Contrib Miner Petrol 171:1–12

Ferroir T (2006) Equation of state and phase transition in KAlSi3O8 hollandite at high pressure. Am Mineral 91:327–332

Fursenko BA, Kholdeyev OV, Litvin YA, Kropachev VD (1986) Apparatus with transparent anvils-windows for optical and X-ray analysis under high pressure. USSR Rept Eng Equip JPRS UEQ 5:80–81

Gianola O, Bartoli O, Ferri F, Galli A, Ferrero S, Capizzi LS, Liebske C, Remusat L, Poli S, Cesare B (2020) Anatectic melt inclusions in ultra-high temperature granulites. J Metamorph Geol 3:321–342

Hwang SL, Shen PY, Chu HT, Yui TF, Liou J, Sobolev NV, Zhang RY, Shatsky VS, Zayachkovsky AA (2004) Kokchetavite: a new potassium-feldspar polymorph from the Kokchetav ultrahigh-pressure terrane. Contrib Miner Petrol 148:380–389

Hwang SL, Yui TF, Chu HT, Shen P, Liou JG, Sobolev NV (2013) Oriented kokchetavite compound rods in clinopyroxene of Kokchetav ultrahigh-pressure rocks. J Asian Earth Sci 63:56–69

Kanzaki M, Xue XY, Amalberti J, Zhang Q (2012) Raman and NMR spectroscopic characterization of high-pressure K-cymrite (KAlSi3O8 center dot H2O) and its anhydrous form (kokchetavite). J Mineral Petrol Sci 107:114–119

Krivovichev SV (2020) FELDSPAR POLYMORPHS: DIVERSITY, COMPLEXITY, STABILITY. Zapiski RMO (Proceedings Russian Mineralogical Society) CXLIX:16–66

Massonne H-J (1992) Evidence for low-temperature ultrapotassic siliceous fluids in subduction zone environments from experiments in the system K2O MgO Al2O3 SiO2 H2O (KMASH). Lithos 28:421–434

Massonne H-J (2015) Derivation of P–T paths from high-pressure metagranites — examples from the Gran Paradiso Massif, western Alps. Lithos 226:265–279

Mikhno AO, Schmidt U, Korsakov AV (2013) Origin of K-cymrite and kokchetavite in the polyphase mineral inclusions from Kokchetav UHP calc-silicate rocks: evidence from confocal Raman imaging. Eur J Mineral 25:807–816

Nicoli G, Gresky K, Ferrero S (2022) Mesoarchean melt and fluid inclusions in garnet from the Kangerlussuaq basement. Southeast Greenl Mineralogia 53:1–9

Petříček V, Dušek M, Palatinus L (2014) Crystallographic Computing System JANA2006: General features. Z für Kristallographie - Crystalline Mater 229:345–352

Romanenko AV, Rashchenko SV, Sokol AG, Korsakov AV, Seryotkin YV, Glazyrin KV, Musiyachenko K (2021) Crystal structures of K-cymrite and kokchetavite from single-crystal X-ray diffraction. Am Mineral 106:404–409

Romanenko AV, Rashchenko SV, Korsakov AV, Sokol AG, Kokh KA (2024) Compressibility and pressure-induced structural evolution of kokchetavite, hexagonal polymorph of KAlSi3O8, by single-crystal X-ray diffraction. Am Mineral 109:1284–1291

Rothkirch A, Gatta GD, Meyer M, Merkel S, Merlini M, Liermann H-P (2013) Single-crystal diffraction at the Extreme conditions beamline P02.2: procedure for collecting and analyzing high-pressure single-crystal data. J Synchrotron Radiat 20:711–720

Schönig J, von Eynatten H, Meinhold G, Lünsdorf NK, Willner AP, Schulz B (2020) Deep subduction of felsic rocks hosting UHP lenses in the central Saxonian Erzgebirge: implications for UHP terrane exhumation. Gondwana Res 87:320–329

Seki Y, Kennedy GC (1964) The breakdown of potassium feldspar, KAlSi3O8 at high temperatures and high pressures. Am Mineral 49:1688–1706

Sheldrick GM (2015) SHELXT– Integrated space-group and crystal-structure determination. Acta Crystallogr Sect Found Adv 71:3–8

Shen G, Wang Y, Dewaele A, Wu C, Fratanduono DE, Eggert J, Klotz S, Dziubek KF, Loubeyre P, Fat'yanov OV (2020) and others Toward an international practical pressure scale: A proposal for an IPPS ruby gauge (IPPS-Ruby2020). High Pressure Research, 40, 299–314

Sokol AG, Kupriyanov IN, Seryotkin YV, Sokol EV, Kruk AN, Tomilenko AA, Bul'bak TA, Palyanov YN (2020) Cymrite as mineral clathrate: an overlooked redox insensitive transporter of nitrogen in the mantle. Gondwana Res 79:70–86

Sokol AG, Kupriyanov IN, Kotsuba DA, Korsakov AV, Sokol EV, Kruk AN (2023) Nitrogen storage capacity of phengitic muscovite and K-cymrite under the conditions of hot subduction and ultra high pressure metamorphism. Geochim Cosmochim Acta 355:89–109

Stähle V, Chanmuang N, Schwarz C, Trieloff WH, M., and, Varychev A (2022) Newly detected shock-induced high-pressure phases formed in amphibolite clasts of the suevite breccia (Ries impact

crater, Germany): Liebermannite, Kokchetavite, and other ultra-high-pressure phases. Contrib Miner Petrol 177:80

Takeuchi Y, Donnay G (1959) The crystal structure of hexagonal CaAl $_2$ Si $_2$ O $_8$. Acta Crystallogr A 12:465–470

Thompson P, Parsons I, Graham CM, Jackson B (1998) The breakdown of potassium feldspar at high water pressures. Contrib Miner Petrol 130:176–186

Wannhoff I, Ferrero S, Borghini A, Darling R, O'Brien PJ (2022) First evidence of dmisteinbergite (CaAl2Si2O8 polymorph) in high-grade metamorphic rocks. Am Mineral 107:2315–2319

Wojdyr M (2010) Fityk: a general-purpose peak fitting program. J Appl Crystallogr 43:1126–1128

Zolotarev AA, Krivovichev SV, Panikorovskii TL, Gurzhiy VV, Bocharov VN, Rassomakhin MA (2019) Dmisteinbergite, CaAl2Si2O8, a metastable polymorph of Anorthite: crystal-structure and Raman Spectroscopic Study of the Holotype Specimen. Minerals 9:570